Control of a Six-axis Robotic Arm Using the Touch Panel

Shyh-Shing Perng[1] , Pu-Sheng Tsai[2], Nien-Tsu Hu[3], Ter-Feng Wu[1], Jen-Yang Chen[4]

[1] Department of Electrical Engineering, National Ilan University, Taiwan
[2] Department of Electronic Engineering, China University of Science and Technology, Taiwan
[3] Chemical Systems Research Division, National Chung-Shan Institute of Science and Technology, Taiwan
[4] Department of Electronic Engineering, Ming Chuan University, Taiwan
ssperng@ems.niu.edu.tw, tsaipusheng@cc.cust.edu.tw, nientsu.hu@gmail.com, tfwu@niu.edu.tw, jychen@mail.mcu.edu.tw

Abstract

The touch panel used for this experiment is the WEINTECH MT6071iE. The six-axis robotic arm was controlled by an AT90CAN128, manufactured by the ATMEL Company. A DGServo servomotor was used to drive the robots joints, which consisted of four servomotors with 12 kg torque, two 1.8 kg servomotors with reduction gear, and some precision aluminum alloy components. Driven by the servomotors, the robotic arm was able to perform motions like fetching, pinching, catching, and releasing. For example, the robotic arm was able to clamp table tennis balls and carry coke cans. In this paper, the D–H method is adopted to set the relative position coordinates of all the joints and connecting rods of the robot arm, and the terminal coordinates of the robotic arm were deduced by combining the degree of freedom with the mechanical limitation of existing arms in accordance with forward kinematics. The results of the D–H method derivation and the actual control results of the robotic arm were compared and the source of error was discussed.

Keywords: Touch panel, Six-axis robotic arm, Servo motor, D-H method, Forward kinematic

1 Introduction

The definition of an industrial robot given by the International Federation of Robotics is that it can be reprogrammed, equipped with multi-function robotic arms [1-5], and is able to carry material, parts, tools, or other special devices by performing various designed motions [6-7]. Industrial robots are mainly utilized in various manufacturing plants. They perform functions, such as panel and wafer welding, assembling, carrying, and packaging. Robotic arms are the form an essential function for industrial robots. Robotic arms are able to imitate the function of human arms, i.e. linear and spatial translation in two-dimensional or three-dimensional space. Robotic arms are commonly comprised of four parts: the mechanical body, controller, servomotor, and sensor. With the main objective of completing wrist and hand movements, they can correctly repeat countless processes once the operator inputs the action sequences according to operational requirements. Derived from hostile environment, the research and development of mechanical arms is beneficial for laborsaving, reducing the risk of exposure to a hazardous work environment, precision manufacturing, and auxiliary operation. For example, in the harsh environment of an atomic energy laboratory, operating machinery is sometimes necessary to deal with radioactive material, when it is deemed unsafe for human beings. The U.S military also used small robots in hazardous areas to remove bombs in Iraq. Prior to robots being used for bomb removal, bomb-disposal experts had to deactivate bombs, which was potentially life threatening. Currently, bomb-disposal robots stand on the frontline instead of experts, which greatly reduces the risk associated with deactivating bombs. The robotic arm is also used in medicine, such as the da Vinci surgical system [8-9], which is composed of a robotic arm system, surgical platform, and micro image display system. It is the most advanced medical surgical system. Through 3D stereo ultra-high resolution images, the human body tissue structures are shown vividly. The robotic arms used for surgical operation imitate the function of the human hand and wrist joint. Through 360 degrees of dexterity, it can conduct fine surgical operations in a narrow space more precisely than a human hand is capable of. The surgical procedure requires a physician. The doctor typically takes a sitting position while performing an operation and accurately removes focal lesions. The use of a robotic arm aids with long, complex operations.

The emergence of technology has managed to witness the evolvement of a new era known as the Internet of Things (IoT). The Internet of Things (IoT) further describes the internetworking of physical devices, vehicles, buildings, and other items which

*Corresponding Author: Shyh-Shing Perng; E-mail: ssperng@ems.niu.edu.tw
DOI: 10.3966/160792642020032102009

include electronics, software, sensors, actuators, and network connectivity that allow these objects to collect and exchange data. The current revolution of IoT coupled with the growing usage of robots in daily activities have turned the Internet of Robotics Things (IoRT) applications into a tangible reality in the nearest future. The advantage of IoRT is that it allows robotic systems to connect, share, and pass the distributed computation resources, business activities, context information, and environmental data with each other.

The objective of this paper is to combine a touch panel with a robotic arm, thereby constructing a complete human–machine interface control system. There are three motivations: (1) To deeply understand how to analyze the motion model of a robotic arm using the DH algorithm [10-11], and to deduct a theoretical formula of forward kinematics and inverse kinematics, thereby establishing the relationship between the movement angle of various joints of an RRR robotic arm and the 3D position coordinates of the end effector of robotic arm, in order to increase the feasibility of robotic arms. (2) To add to the function of embedded micro controller, thereby increasing the likelihood of feasibility of the mechanical arm. This paper adopted the embedded micro controller AT90CAN128 as the control core chip. It has six sets of PWM output signals, which can directly drive six joint servomotors, and a group of UART serial communications to communicate with the touch panel. Given the perfect integration of the micro control chip and touch panel, the human-machine interface control of the end effector of the robotic arm can be achieved. (3) To embed a wireless transmission module and improve the remote-control ability. As mentioned above, the development of robotic arms was originally motivated to aide with harsh environmental requirements.

2 Movement Model of Robotic Arms

The six-axis robotic arm was designed based on the structure of the human arm, as shown in Figure 1. It comprised of six components: a base joint, shoulder joint, elbow joint, bending wrist joint, rotary wrist joint, and finger joint. Each joint is driven by a servo motor. The position and direction of the end of the robotic arm is calculated using robot kinematics. Since the robotic arm is a set of linkages connected with joints, the degree of freedom is the total degree of freedom (DOF) of all the links before connection and fixation, subtracted by the constraint degree of all the joints and the degree of freedom of the fixed links. The number of the DOF is directly related to the motion of the robotic arms. For example, with one DOF, the arm can only move in one direction.

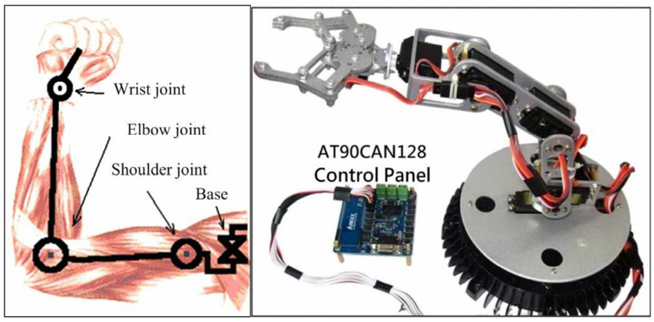

Figure 1. Structure of the human arm and the six-axis robotic arm

The objective of this paper is to determine the position of the end effector in 3D Euclidean space, otherwise known as the coordinates of the wrist joint. Since the posture of rotation is not in the scope of this paper, the rotating wrist joint and finger joints for clipping will not be given consideration. Thus, the six-axis robotic arm has four DOFs from the base joint, shoulder joint, elbow joint, and bending wrist joint. Denavit and Hartenberg (simplified as D–H) proposed a general method in 1954 to express the geometric relationship of bars in space for robotic kinematics, which is widely employed. In this paper, the D–H coordinate system was adopted. Proper D–H four-link parameters were then defined according to planar RRR six-axis robotic arms, thereby transforming a complicated coupling relationship to a simple transform relationship of a homogeneous matrix.

2.1 Transmitting Board for the Wearable Device

2.1.1 Establishment of the Coordinate System

As shown in Figure 2, joint i connects rods i-1 and i. A rigid body coordinate system must be established on each joint. The i th coordinate system must be determined based on the posture of the previous coordinate system, i-1. The coordinate systems were established following the rules below:

(1) The axis of joint i is defined as the z_i axis of the coordinate system.

(2) The common perpendicular line between z_i and z_{i-1} is defined as the x_i axis of coordinate system.

(3) The crossover point between the x_i axis and z_i axis is defined as the origin of the *ith* coordinate system.

(4) The y_i axis is then defined based on the right-hand rule.

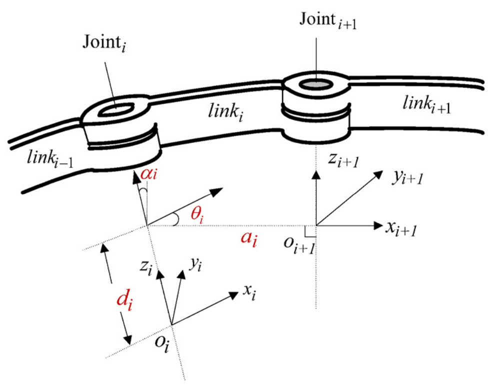

Figure 2. Definition of the D–H coordinate system and the four-link parameters

Figure 2 Definition of the D–H coordinate system and the four-link parameters

2.1.2 Parameter Setting of the D-H method

Comparing the $\{i\}_{\text{th}}$ coordinate system and the $\{i+1\}_{\text{th}}$ coordinate system, the rotation angle of each joint and the distance between each connecting rod constitute the four-link parameters of the D–H method, namely, d_i, a_i, α_i and θ_i. Specifically, d_i also called as rod spacing, is the distance between O_i and O_{i+1} in the z_i direction. a_i, also called the rod length, is the distance between O_i and O_{i+1} in the x_i direction. α_i is the angle of rotation by moving z_i to z_{i+1} along x_i. θ_i, also called as joint rotation, is the angle of rotation by moving x_i to x_{i+1} along z_i. For a rotating joint, θ_i is a variable. For a translational or sliding joint, d_i is a variable.

(1) The joint rotation, θ_i is angle of rotation by moving x_i to x_{i+1} along z_i. The homogeneous transformation matrix between the two coordinate systems is expressed as:

$$R(z,\theta)=\begin{bmatrix} c\theta_i & -s\theta_i & 0 & 0 \\ s\theta_i & c\theta_i & 0 & 0 \\ 0 & 0 & 1 & 0 \\ 0 & 0 & 0 & 1 \end{bmatrix} \quad \textbf{(1)}$$

For convenience, $\cos(\theta_i)$ is simplified as $c\theta_i$ and $\sin(\theta_i)$ is simplified as $s\theta_i$.

(2) The rod spacing, d_i is the distance between O_i and O_{i+1} in z_i direction. The homogeneous transformation matrix between the two coordinate systems is expressed as:

$$T(z,d)=\begin{bmatrix} 1 & 0 & 0 & 0 \\ 0 & 1 & 0 & 0 \\ 0 & 0 & 1 & d_i \\ 0 & 0 & 0 & 1 \end{bmatrix} \quad \textbf{(2)}$$

(3) The rod length a_i is the distance between O_i and O_{i+1} in x_i direction. The homogeneous transformation matrix between the two coordinate systems is expressed as:

$$T(x,a)=\begin{bmatrix} 1 & 0 & 0 & a_i \\ 0 & 1 & 0 & 0 \\ 0 & 0 & 1 & 0 \\ 0 & 0 & 0 & 1 \end{bmatrix} \quad \textbf{(3)}$$

(4) α_i is the angle of rotation by moving z_i to z_{i+1} along x_i. The homogeneous transformation matrix between the two coordinate systems is expressed as:

$$R(x,\alpha)=\begin{bmatrix} 1 & 0 & 0 & 0 \\ 0 & c\alpha_i & -s\alpha_i & 0 \\ 0 & s\alpha_i & c\alpha_i & 0 \\ 0 & 0 & 0 & 1 \end{bmatrix} \quad \textbf{(4)}$$

Based on the above four transformation matrices, the D-H coordinate transformation matrix from the $\{i\}_{\text{th}}$ coordinate system and the $\{i+1\}_{\text{th}}$ coordinate system can be expresses as:

$$^{i+1}_{\ \ i}A = R(z,\theta)T(z,d)T(x,a)R(x,\alpha) \quad \textbf{(5)}$$

$$=\begin{bmatrix} c\theta_i & -s\theta_i c\alpha_i & s\theta_i s\alpha_i & a_i c\theta_i \\ s\theta_i & c\theta_i c\alpha_i & -c\theta_i s\alpha_i & a_i s\theta_i \\ 0 & s\alpha_i & c\alpha_i & d_i \\ 0 & 0 & 0 & 1 \end{bmatrix} \quad \textbf{(6)}$$

The D–H homogeneous matrix from the $\{0\}$ coordinate system to the $\{i+1\}$ coordinate system can be expressed as:

$$^{i}_{0}A = {}^{1}_{0}A\ {}^{2}_{1}A\ {}^{3}_{2}A \cdots {}^{\ i}_{i-1}A = \prod_{j=1}^{i} {}^{\ j}_{j-1}A \quad \textbf{(7)}$$

2.2 Forward Kinematics

In forward kinematics, the position coordinate of the end effector is calculated based on the known axis movement angle of each joint in three-dimensional space. Figure 3 shows the structure and appearance of the six-axis robotic arm. The coordinate systems and related parameters are shown on the left side. In order to simplify the design of this system, it is assumed that the base is fixed without arbitrary rotation, so the rigid axis on the base is always in the same direction. In other words, the robotic arm will only move in one plane, which is referred to as a planar RRR robotic arm. In addition, posture control is not in the scope of this paper, so the finger joint and the rotating wrist joint is not discussed. Figure 4 is the dimensional diagram of the six-axis robotic arm used in this study with an arm length of 390 mm, a maximum weight of 200 g, and a base disc diameter of 210 mm.

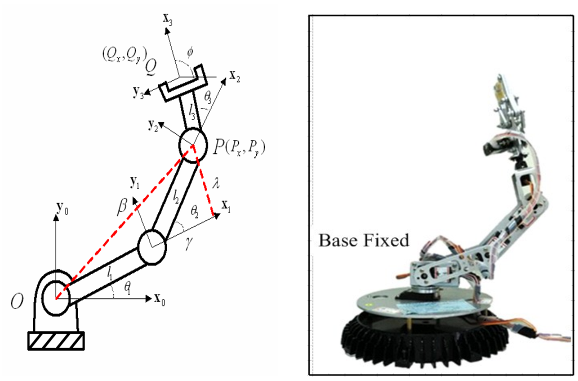

Figure 3. Base-fixed planar RRR four-axis robotic arm

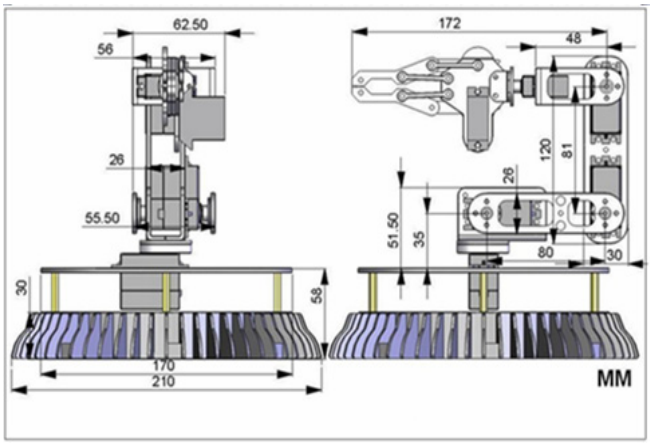

Figure 4. Dimensions of the six-axis robotic arm

The motion equation of the six-axis robotic arm is deduced based on the D-H method. Only the shoulder joint, elbow joint, and bending wrist joint were considered in this study. First, the D-H four-link parameters of each joint were established. The four D-H linkage parameters are shown in Table 1.

Table 1. D-H four-link parameters

Joint (i)	α_i Twist Angle	a_i Rod Length	θ_i Joint Angle	d_i displacement
1	0	l_1	θ_1	0
2	0	l_2	θ_2	0
3	0	l_3	θ_3	0

By substituting the parameters from Figure 1 into (6), it follows that:

$$
{}^{1}_{0}A=\begin{bmatrix} c\theta_1 & -s\theta_1 & 0 & l_1 c\theta_1 \\ s\theta_1 & c\theta_1 & 0 & l_1 s\theta_1 \\ 0 & 0 & 1 & 0 \\ 0 & 0 & 0 & 1 \end{bmatrix},\ {}^{2}_{1}A=\begin{bmatrix} c\theta_2 & -s\theta_2 & 0 & l_2 c\theta_2 \\ s\theta_2 & c\theta_2 & 0 & l_2 s\theta_2 \\ 0 & 0 & 1 & 0 \\ 0 & 0 & 0 & 1 \end{bmatrix},
$$

$$
{}^{3}_{2}A=\begin{bmatrix} c\theta_3 & -s\theta_3 & 0 & l_3 c\theta_3 \\ s\theta_3 & c\theta_3 & 0 & l_3 s\theta_3 \\ 0 & 0 & 1 & 0 \\ 0 & 0 & 0 & 1 \end{bmatrix} \tag{8}
$$

Based on (7), the transformation coordinates from {0} to {2} and {3} are:

$$
{}^{2}_{0}A={}^{1}_{0}A\cdot{}^{2}_{1}A=\begin{bmatrix} c\theta_1 c\theta_2 - s\theta_1 s\theta_2 & -c\theta_1 s\theta_2 - s\theta_1 c\theta_2 & 0 & l_1 c\theta_1 + l_2 c\theta_{12} \\ s\theta_1 c\theta_2 + c\theta_1 s\theta_2 & -s\theta_1 s\theta_2 + c\theta_1 c\theta_2 & 0 & l_1 s\theta_1 + l_2 s\theta_{12} \\ 0 & 0 & 1 & 0 \\ 0 & 0 & 0 & 1 \end{bmatrix} \tag{9}
$$

$$
{}^{3}_{0}A={}^{2}_{0}A\cdot{}^{3}_{2}A=\begin{bmatrix} c\theta_{123} & -s\theta_{123} & 0 & l_1 c\theta_1 + l_2 c\theta_{12} + l_3 c\theta_{123} \\ s\theta_{123} & c\theta_{123} & 0 & l_1 s\theta_1 + l_2 s\theta_{12} + l_3 s\theta_{123} \\ 0 & 0 & 1 & 0 \\ 0 & 0 & 0 & 1 \end{bmatrix} \tag{10}
$$

Herein,

$$
c\theta_{12}=\cos(\theta_1+\theta_2),\ c\theta_{123}=\cos(\theta_1+\theta_2+\theta_3).
$$

Forward kinematics is used to derive the homogeneous matrix of the whole structure, including the posture and position vectors of the arm, as shown in (11). The 3 / 3 r elements in the top left matrix is the rotation matrix, or posture matrix, and Q_x, Q_y and Q_z, on the right are the position vectors. The position and posture after movement is obtained by applying the homogeneous matrix.

$$
{}^{i}_{0}A={}^{1}_{0}A\ {}^{2}_{1}A\ {}^{3}_{2}A\ \cdots\ {}^{i}_{i-1}A
=\prod_{j=1}^{i}{}^{j}_{j-1}A=\begin{bmatrix} r_{11} & r_{12} & r_{13} & Q_x \\ r_{21} & r_{22} & r_{23} & Q_y \\ r_{31} & r_{32} & r_{33} & Q_z \\ 0 & 0 & 0 & 1 \end{bmatrix} \tag{11}
$$

According to the above discussion, the coordinates of the center point of the rotating wrist joint can be calculated by (10).

$$
Q_x=l_1\cos\theta_1+l_2\cos(\theta_1+\theta_2)+l_3\cos(\theta_1+\theta_2+\theta_3) \tag{12}
$$

$$
Q_y=l_1\sin\theta_1+l_2\sin(\theta_1+\theta_2)+l_3\sin(\theta_1+\theta_2+\theta_3) \tag{13}
$$

The coordinates of the center point of the bending wrist joint can be calculated by (9).

$$P_x = l_1 \cos\theta_1 + l_2 \cos(\theta_1 + \theta_2) \quad \textbf{(14)}$$

$$P_y = l_1 \sin\theta_1 + l_2 \sin(\theta_1 + \theta_2) \quad \textbf{(15)}$$

2.3 Inverse Kinematics

According to inverse kinematics, the rotation angle of each joint is calculated based on known spatial coordinates, Q, of the end effector of the robotic arm. Figure 5 shows a base-fixed planar RRR four-axis robotic arm on the left side.

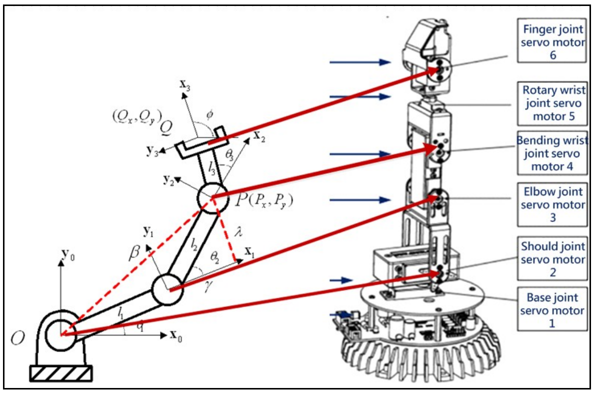

Figure 5. Inverse kinematics

Assuming that the coordinates of the center point of the rotating wrist joint are (Q_x, Q_y), the coordinates of the center point of the bending wrist joint are (P_x, P_y), and the orientation angle of the end of the robotic arm is ϕ, the joint angles θ_1, θ_2, θ_3 were calculated. The orientation angle of the end of the robotic arm is defined as:

$$\theta_{123} = \theta_1 + \theta_2 + \theta_3 = \phi \quad \textbf{(16)}$$

The relationship between the coordinates of the rotating joint, Q, and the coordinates of the bending wrist joint, P, can be expressed as:

$$P_x = Q_x - l_3 \cos(\phi) = l_1 \cos\theta_1 + l_2 \cos(\theta_1 + \theta_2) \quad \textbf{(17)}$$

$$P_y = Q_y - l_3 \sin(\phi) = l_1 \sin\theta_1 + l_2 \sin(\theta_1 + \theta_2) \quad \textbf{(18)}$$

For convenience, the four-axis robotic arm is simplified into a three-axis robotic arm. Based on the coordinates of the bending wrist joint (P_x, P_y), the rotation angle of each joint is calculated using inverse kinematics. From Figure 5, it can be observed that:

$$\beta^2 = P_x^{\ 2} + P_y^{\ 2}, \ \lambda = l_2 \sin\theta_2, \ \gamma = l_2 \cos\theta_2 \quad \textbf{(19)}$$

It can be further simplified to:

$$\begin{aligned}\beta^2 &= \lambda^2 + (l_1 + \gamma)^2 = (l_2 \sin\theta_2)^2 + [l_1 + (l_2 \cos\theta_2)]^2 \\ &= l_1^2 + l_2^2 + 2 l_1 l_2 \cos\theta_2\end{aligned} \quad \textbf{(20)}$$

Therefore, the rotation angle, θ_2 of the elbow joint is obtained from (19) and (20).

$$\theta_2 = \cos^{-1}\left(\frac{P_x^2 + P_y^2 - l_1^2 - l_2^2}{2 l_1 l_2}\right) \quad \textbf{(21)}$$

From (11), although both P_x and P_y contain positive and negative values, the rod length l_1 and l_2 remain positive. In the area range of θ_2 which the robotic arm can reach, θ_2 calculated by (11) will be positive. The negative sign of θ_2 can only be determined based on the values of P_x and P_y. The following situations will be discussed:

(1) When $\left|P_x^2 + P_y^2 - l_1^2 - l_2^2\right| < 1$ $0 < \theta_2 < 90^0$ or $-90^o <$ $\theta_2 < 0^0$

(2) When $\left|P_x^2 + P_y^2 - l_1^2 - l_2^2\right| = 1$, the robotic arm is either in the state of extension or in a folded condition.

(3) When $\left|P_x^2 + P_y^2 - l_1^2 - l_2^2\right| > 1$, the robotic arm is not able to reach the position.

The angle range of the servo motors used in the system is $0 < \theta_2 < 60^0$ or $-60^o < \theta_2 < 0^0$. In other words, only when the following conditions $0.5 < P_x^2 + P_y^2 - l_1^2 - l_2^2 < 1$ and $-1 < P_x^2 + P_y^2 - l_1^2 - l_2^2 < -0.5$ are satisfied, can the robotic arm reach the position.

Then, the rotation angle, θ_1 of the elbow joint is deducted according to (14) and (15).

$$P_x = l_1 \cos(\theta_1) + l_2 \cos(\theta_1 + \theta_2) \quad \textbf{(22)}$$

$$P_y = l_1 \sin(\theta_1) + l_2 \sin(\theta_1 + \theta_2) \quad \textbf{(23)}$$

Based on the product to sum formula, (14) and (15) can be simplified as:

$$P_x = l_1 \cos\theta_1 + l_2 \cos\theta_1 \cos\theta_2 - l_2 \sin\theta_1 \sin\theta_2 \quad \textbf{(24)}$$

$$P_y = l_1 \sin\theta_1 + l_2 \sin\theta_1 \cos\theta_2 + l_2 \cos\theta_1 \sin\theta_2 \quad \textbf{(25)}$$

It can be further simplified as:

$$P_x = (l_1 + l_2 \cos\theta_2)\cos\theta_1 - (l_2 \sin\theta_2)\sin\theta_1 \quad \textbf{(26)}$$

$$P_y = (l_2 \sin\theta_2)\cos\theta_1 + (l_1 + l_2 \cos\theta_2)\sin\theta_1 \quad \textbf{(27)}$$

Assuming $\cos\theta_1$ and $\sin\theta_1$ are two unknown variables, and (26) and (15) are dual linear equations, then

$$\sin\theta_1 = \frac{(l_1 + l_2 \cos\theta_2)P_y - (l_2 \sin\theta_2)P_x}{(l_1 + l_2 \cos\theta_2)^2 + (l_2 \sin\theta_2)^2} \quad \textbf{(28)}$$

$$\cos\theta_1 = \frac{(l_1 + l_2 \cos\theta_2)P_x + (l_2 \sin\theta_2)P_y}{(l_1 + l_2 \cos\theta_2)^2 + (l_2 \sin\theta_2)^2} \quad \textbf{(29)}$$

the rotation angle of the elbow joint is:

$$\theta_1 = \tan^{-1}\left(\frac{(l_1 + l_2 \cos\theta_2)P_y - (l_2 \sin\theta_2)P_x}{(l_1 + l_2 \cos\theta_2)P_x + (l_2 \sin\theta_2)P_y}\right) \quad \textbf{(30)}$$

Once θ_1 and θ_2 are obtained by (21) and (30), the rotation angle of the bending wrist joint is:

$$\theta_3 = \phi - \theta_1 - \theta_2 \tag{31}$$

Herein, $\phi = \tan^{-1} Q_y / Q_x$.

3 System Architecture of the Six-axis Robotic Arm

The primary objective for this system is to use an embedded microprocessor and touch panel as the main control platform, along with an ATMEL microcontroller as the core chip, in order to completely control the six-axis robotic arm. As this solution is different from traditional personal computer control platforms, it can greatly reduce the system cost and has the advantage of portability. Figure 6 shows the structure of the system. The system consists of a six-axis robotic arm, a WEINTEK touch panel, and an AT90CAN128 core chip PWM control panel.

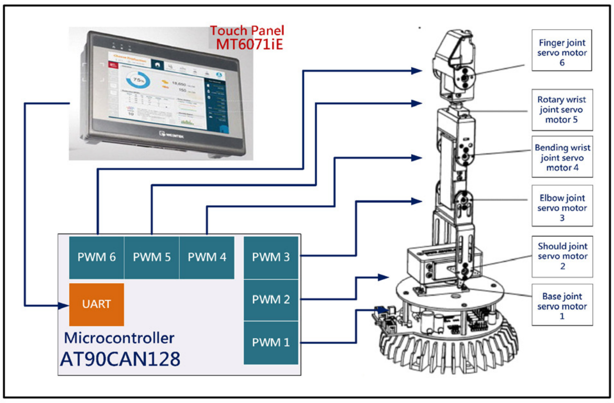

Figure 6. System architecture of the six-axis robotic arm

Figure 7 shows the structure of the robotic arm used in this study. The mechanical specifications are: (1) net weight: 2 kg, (2) arm length: 390 mm, (3) maximum distance of claw: 53 mm, (4) two Micro STD servo motors with 1.8 kg torque, (5) four metal gear servo motors with 12 kg torque, (6) 6 DOFs, (7) maximum lifting force: 200 g (at 6 V / 3 A working voltage), (8) aluminum alloy structure with super metal texture, which is scratch proof on the surface of aluminum parts. The electrical specifications are: (1) working voltage 4.8-6 V, (2) power consumption of servo motors: 2-3 A, (3) control core chip AT90CAN128. The mechanical arm is composed of six servo motors (including a reduction gearbox reducer and a PID control circuit), which correspondingly control the rotation of the base joint, lift of the shoulder joint, swing of the elbow joint, rotation and bending of the wrist joint, and clamping of the finger joint. The base, shoulder, elbow, and rotating wrist joints are driven by 12 kg torque metal gear servo motors, while the bending wrist and finger joints are driven by 1.8 kg torque servo motors. The characteristics of the metal gear servo motor are as follows: (1) dimensions: 40.4 x 9.8 x 36 mm, (2) weight: 48 g, (3) speed: 0.22 sec/60°, (4) output torque: 12 kg-cm. In addition, the characteristics of the DGServoS05NF STD servo motors are: (1) dimensions: 28 / 14 / 59.8 mm, (2) weight: 18 g, (3) speed: 0.13 sec/60°, (4) output torque: 1.8 kg-cm. Rubber pads were assembled in the inner side of the fixture in order to increase the grasping friction. Figure 7 shows the specifications of the six-axis robotic arm. Figure 8 shows the fixture of finger joint.

Figure 7. Specifications of the six-axis robotic arm

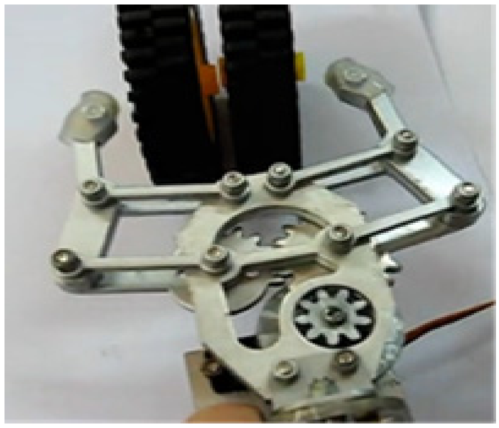

Figure 8. Fixture of finger joint

4 Tests and Results

4.1 Tests of Six-axis Joint Motors

Figure 9 shows the position of the six-axis robotic arm when the base joint, shoulder joint, elbow joint, bending wrist joint, rotating wrist joint, and finger joint rotate -60°, -60°, 50°, -20°, 0°, and 30°, respectively. Figure 10 shows the position of the arm when the base joint, shoulder joint, elbow joint, bending wrist joint, rotating wrist joint, and finger joint rotate 30°, -60°, 50°, -20°, 0°, and 30°, respectively. The difference between the two conditions is that the base joint moves to the left by 60° in the first condition, while it moves to the right by 30° in the second. Figure 11 shows the position of the arm when the base joint, shoulder joint, elbow joint, bending wrist joint, rotating wrist joint, and finger joint rotate 30°, 30°, 50°, -20°, 0°, and 30°, respectively.

Figure 9. Test (I) of the six-axis joint motors

Figure 10. Test (II) of the six-axis joint motors

Figure 11. Test (III) of the six-axis joint motors

4.2 Integration Test

In this section, an integration test is described. Specifically, two tests were conducted. In the first test, the aim was to move the end effector (rotating wrist joint) and bending wrist joint to the following coordinate position:

(P_x =120mm, P_y = 105mm, Q_x = 135mm, Q_y = 150mm)

In the second test, the aim was to move the end effector (rotating wrist joint) and bending wrist joint to the following coordinate position:

(P_x =-138mm, P_y = 158.9mm, Q_x = -175mm, Q_y = 95mm)

On the human-machine interface of the WEINTEK touch panel MT6071iE, when the button "inverse kinematics" is pressed, a window (as shown in Figure 12) will pop up. In the window, the coordinates of the bending wrist joint (P_x, P_y) and the rotating wrist joint (Q_x, Q_y) can be entered. Pressing the button "Calculation of inverse kinematics" displays that the angle of the shoulder joint motor θ1 = 33°, the angle of the elbow joint motor θ2 = 16°, and angle of the bending wrist joint motor θ3 = 22, as shown in Figure 12.

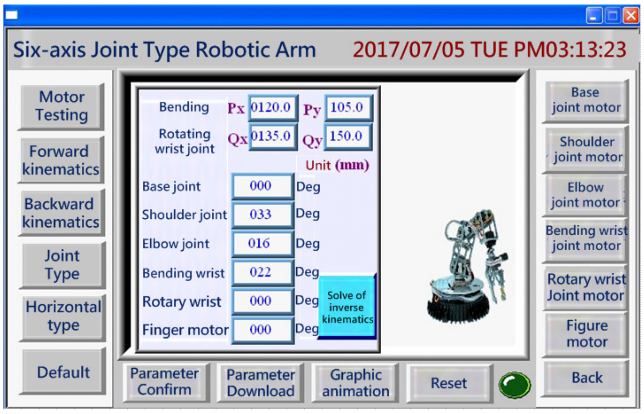

Figure 12. Results of the first test from inverse kinematics

Similarly, in the second test, it is obtained that the angle of shoulder joint θ1 = -43°, the elbow joint θ2 = 34°, and bending wrist joint θ3 = -30°, as shown in Figure 13.

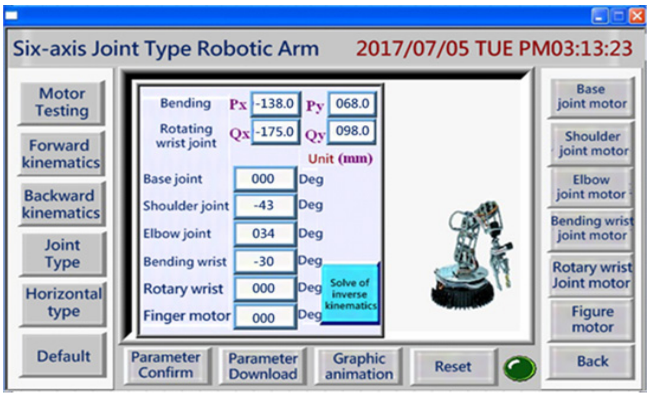

Figure 13. Results of the second test from inverse kinematics

In the second step, by pressing the button "download parameters", the WEINTEK MT6071iE sends the movement angle data of every joint to the motor drive board AT90CAN128 via an RS232 serial communication port. The micro controller then generates a PWM pulse modulation signal to drive the six-axis robotic arm towards the target position. Once the robotic arm reaches the position, the coordinates of points Q and P are measured with a ruler.

The measured coordinates of the first test are: (as shown in Figure 14, Figure 15 and Table 2).

$$P(P_x = 119.5mm,\ P_y = 108mm) 、$$
$$Q(Q_x = 134.5mm,\ Q_y = 149.5mm).$$

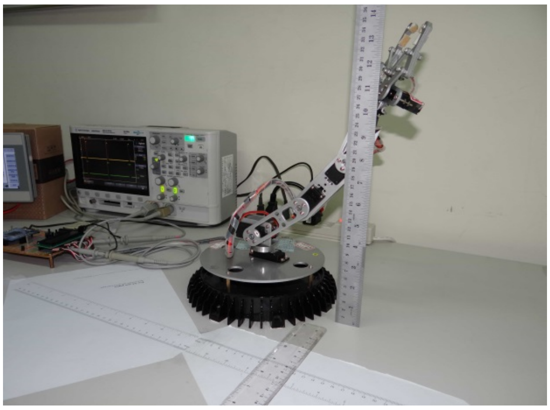

Figure 14. Coordinate measurement of Point P in the first test

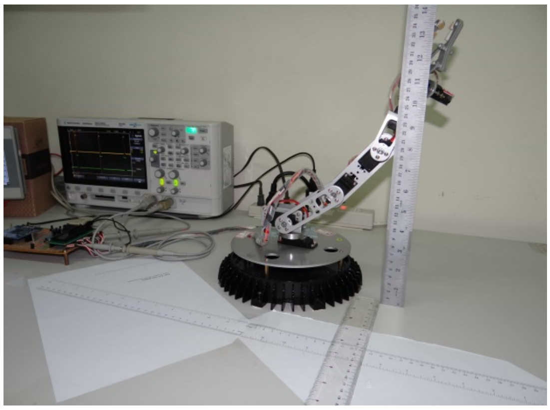

Figure 15. Coordinate measurement of Point Q in the first test

Table 2. Comparison of the theoretical and measurement values of the coordinates of P and Q in the first test

Theoretic value			Ideal value/Actual vale/Error value											
Shoulder	Elbow	Bending wrist	Wrist joint (P)						Wrist joint (Q)					
θ1 (deg)	θ2 (deg)	θ3 (deg)	Px Ideal value	Px Actual value	Px Error	Py Ideal value	Py Actual value	Py Error	Qx Ideal value	Qx Actual value	Qx Error	Qy Ideal value	Qy Actual value	Qy Error
33	16	22	120.0	119.5	0.5	105.0	108.0	-3	135.0	134.5	0.5	150.0	149.5	0.5

The measured coordinates of the second test are: (as shown in Figure 16, Figure 17 and Table 3).

$$P(P_x = -138mm,\ P_y = 68mm) 、$$
$$Q(Q_x = -175mm,\ Q_y = 98mm)$$

5 Conclusions

In the current study, the robotic arm is comprised of six joints, which are powered by six servomotors (including reduction gear and a PID control circuit). The servomotors perform the rotation of the base joint, lifting of the shoulder joint, swing of the elbow joint, rotation and bending of the wrist joint, and grasping of the finger joint. The primary objective of this system is to use an embedded microprocessor and a touch panel as the main control platform, along with an ATMEL microcontroller as the core chip, in order to have full control of the six-axis robotic arm. As this system is different from the traditional personal computer control platform, it can greatly reduce the system cost, and has the advantage of portability. Currently, using the third generation AT90CAN128 chip as the micro controller meets the current working requirement. However, it might be unable to cope with the calculation work if given more functions. In future work, the AT90CAN128 microcontroller should be replaced with a fourth-generation ARM embedded microprocessor, in order to cope with a heavier computational load. Also, Touch Panel will be developed into an IoT system (including web pages and cloud servers). The Touch Panel can be removed via a mobile phone, laptop or computer to control a six-axis robotic arm.

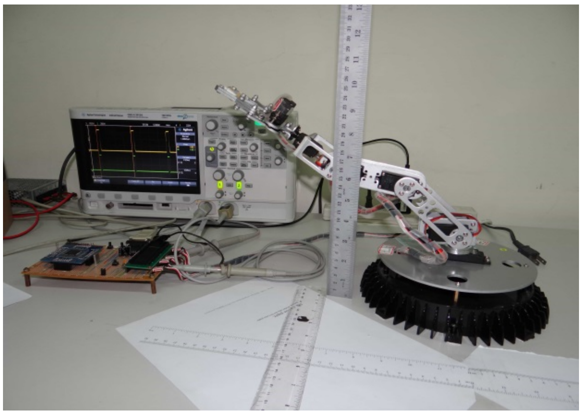

Figure 16. Coordinate measurement of Point P in the second test

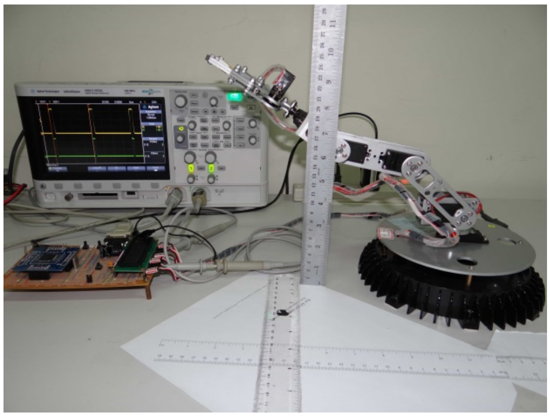

Figure 17. Coordinate measurement of point Q in the second test

Table 3. Comparison of the theoretical and measurement values of the coordinates of P and Q in the second test

Theoretic value			Ideal value/Actual vale/Error value											
Shoulder	Elbow	Bending wrist	Wrist joint (P)						Wrist joint (Q)					
θ1 (deg)	θ2 (deg)	θ3 (deg)	Px Ideal value	Px Actual value	Px Error	Py Ideal value	Py Actual value	Py Error	Qx Ideal value	Qx Actual value	Qx Error	Qy Ideal value	Qy Actual value	Qy Error
-44	35	-29	-137.5	-138.0	0.5	68.0	68.0	0.0	175.0	175.0	0.0	97.8	95.0	2.8

References

[1] M. Zhong, Y. Zhang, X. Yang, Y. Yao, J. Guo, Y. Wang, Y. Liu, Assistive Grasping Based on Laser-point Detection with Application to Wheelchair- mounted Robotic Arms, *Sensors*, Vol. 19, No. 2, pp. 1-14, January, 2019.

[2] P. Lucibello, Repositioning Control of Robotic Arms by Learning, *IEEE Transactions on Automatic Control*, Vol. 39, No. 8, pp. 1690-1694, August, 1994.

[3] Y. W. Liang, S. D. Xu, D. C. Liaw, C. C. Chen, A Study of T-S Model-Based SMC Scheme with Application to Robot Control, *IEEE Transactions on Industrial Electronics*, Vol. 55, No. 11, pp. 3964-3971, December, 2008.

[4] H. C. Huang, S. S. D. Xu, H. S. Hsu, Hybrid Taguchi DNA Swarm Intelligence for Optimal Inverse Kinematics Redundancy Resolution of Six-DOF Humanoid Robot Arms, *Mathematical Problems in Engineering*, Vol. 2014, pp. 1-9, July, 2014.

[5] H. C. Huang, S. S. D. Xu, C. H. Chiang, Optimal Fuzzy Controller Design Using an Evolutionary Strategy-Based Particle Swarm Optimization for Redundant Wheeled Robots, *International Journal of Fuzzy Systems*, Vol. 17, No. 3, pp. 390-398, June, 2015.

[6] T. F. Wu, Tracking Control of Wheeled Mobile Robots Using Fuzzy CMAC Neural Networks, *Journal of Internet Technology*, Vol. 19, No. 6, pp. 1853-1869, November, 2018.

[7] P. S. Tsai, T. F. Wu, N. T. Hu, J. Y. Chen, Obstacle Avoidance System for Wheeled Mobile Robots by CMOS Image Sensor, *Journal of Internet Technology*, Vol. 17, No. 4, pp. 703-710, July, 2016.

[8] Z. Li, I. Tong, L. Metcalf, C. Hennessey, S. E. Salcudean, Free Head Movement Eye Gaze Contingent Ultrasound Interfaces for the da Vinci Surgical System, *IEEE Robotics and Automation Letters*, Vol. 3, No. 3, pp. 2137-2143, July, 2018.

[9] O. Mohareri, M. Ramezani, T. K. Adebar, P. Abolmaesumi, S. E. Salcudean, Automatic Localization of the da Vinci Surgical Instrument Tips in 3-D Transrectal Ultrasound, *IEEE Transactions on Biomedical Engineering*, Vol. 60, No. 9, pp. 2663-2672, September, 2013.

[10] W. Dong, W. Lin, C. Qian, C. Ye, H. Gao, GA-based Modified D-H Method Calibration Modelling for 6-DOFs Serial Robot, *2016 31st Youth Academic Annual Conference of Chinese Association of Automation (YAC)*, Wuhan, China, 2016, pp. 225-230.

[11] S. Wen, Z. Ma, S. Wen, Y. Zhao, J. Yao, The Study of NAO Robot Arm Based on Direct Kinematics by Using D-H Method, *2014 UKACC International Conference on Control (CONTROL)*, Loughborough, UK, 2014, pp. 515-518.

Biographies

Shyh-Shing Perng was born in Taiwan in 1960. He received the B.S. degree in Department of Industrial Education from National Taiwan Normal University, Taipei, Taiwan, in 1984. He received the M.S. degree in Department of Control Engineering from National Chiao Tung University, Hsinchu, Taiwan, in 1991. He received the Ph.D. degree in Department Electrical

Engineering from National Taiwan University of Science and Technology, Taipei, Taiwan, in 1999. He is currently an Associate Professor of the Department of Electrical Engineering, National Ilan University, Yilan, Taiwan. His research interests include motor control, engineering education, green energy, unmanned aerial vehicles (UAVs) and mobile robot, etc.

Pu-Sheng Tsai was born in Taiwan, R.O.C., in 1962. He received the M.S. degree in automatic control from the Feng Chia University, Taichung, Taiwan, R.O.C., in 1985 and the Ph.D. degree in electrical engineering from the National Taiwan University, in 1998. He is currently an Assistant Professor and was a chair in 2017-2018 at the Department of Electronic Engineering, China University of Technology and Science. His research interests are Embedded Micro-controller application, robot control, Artificial Intelligence, Internet of thing and Virtual Reality.

Nien-Tsu Hu is a researcher at National Chung-Shan Institute of Science and Technology in Taiwan. He was born in Tainan, Taiwan in 1979. He received B.S. degree in Electrical Engineering from the Chung Yuan Christian University and M.S. degree in Department of Electrical Engineering from National Taiwan University of Science and Technology in 2001 and 2003, respectively. Since 2003, he has started his graduate study for Ph.D. degree at the Department of Electrical Engineering, National Cheng Kung University, Tainan, Taiwan, R.O.C. and he has received Ph.D. degree in 2010. His research focuses on intelligent control, Embedded System, robot control, optimal control, decentralize control, system identification, and motor servo control.

Ter-Feng Wu was born in Taiwan in 1962. He received the B.S. degree in Department of Industrial Education from National Taiwan Normal University, Taipei, Taiwan, in 1986. He received the M.S. degree in Department of Control Engineering from National Chiao Tung University, Hsinchu, Taiwan, in 1993. He received the Ph.D. degree in Department Electrical Engineering from National Taiwan University, Taipei, Taiwan, in 2006. He is currently a professor and was a chair in 2009-1015 at the Department of Electrical Engineering, National Ilan University, Yilan, Taiwan. His research interests include intelligent control, neural network, fuzzy CMAC, green energy, unmanned aerial vehicles (UAVs) and mobile robot, etc.

Jen-Yang Chen received the M.S. degree in electrical engineering from the Tatung University, Taipei, Taiwan, R.O.C., in 1992 and the Ph.D. in electrical engineering from Tamkang University, in 2000. He is currently a full professor in the Department of Electronic Engineering at Ming Chuan University. His research interests include machine learning, intelligent control, fuzzy and neural network systems, science education.